CENTRIFUGE TESTS ON ROCK-SOCKETED PILES: EFFECT OF SOCKET ROUGHNESS ON SHAFT RESISTANCE

Gutiérrez-Ch J.G.[1*], Song G.[2+], Heron C.M.[3º], Marshall, A.[4º] and Jimenez R.[5*]

ABSTRACT

Preliminary estimations of shaft resistance of rock-socketed piles are usually conducted using empirical formulations which relate to the uniaxial compressive strength (σ_c) of the weaker material involved (intact rock or pile). However, there are other factors, such as the degree of socket roughness, that could affect the shaft resistance of rock-socketed piles. In this paper, results from geotechnical centrifuge tests are presented to demonstrate the effect of socket roughness on the pile shaft resistance. Aluminum model piles with different degrees of shaft roughness were fabricated and embedded within an artificial rock mixture composed of sand, cement, bentonite and water. Pile loading tests were conducted within the centrifuge and axial forces along the model piles were measured using fiber Bragg grating (FBG) sensing technology. Results are used to demonstrate that centrifuge testing provides a suitable experimental method to study and quantify the effect of socket roughness on the shaft shearing mechanism of rock-socketed piles. Finally, the centrifuge test measurements are compared with several formulations published in the literature, suggesting that centrifuge measurements tend to agree with the overall trend, despite the variability of predictions obtained with different formulations.

[1]Research Associate. E-mail: jg.gutierrez@upm.es
[2]Research Associate. E-mail: geyang.song@eng.ox.ac.uk
[3]Associate Professor. E-mail: charles.heron@nottingham.ac.uk
[4]Associate Professor. E-mail: alec.marshall@nottingham.ac.uk
[5]Professor. E-mail: rafael.jimenez@upm.es

*ETSI Caminos, Canales y Puertos, Universidad Politécnica de Madrid. C/Prof. Aranguren, 12, Madrid 28040, Spain.
ºNottingham Centre for Geomechanics, University of Nottingham, University Park NG7 2RD Nottinghamshire, UK.
+ Department of Engineering Science, University of Oxford, Parks Road, Oxford, OX1 3PJ, UK.

Keywords Rock-socketed piles, shaft resistance, socket roughness, centrifuge tests, fiber Bragg grating.

[1]Research Associate. E-mail: jg.gutierrez@upm.es
[2]Research Associate. E-mail: geyang.song@eng.ox.ac.uk
[3]Associate Professor. E-mail: charles.heron@nottingham.ac.uk
[4]Associate Professor. E-mail: alec.marshall@nottingham.ac.uk
[5]Professor. E-mail: rafael.jimenez@upm.es

*ETSI Caminos, Canales y Puertos, Universidad Politécnica de Madrid. C/Prof. Aranguren, 12, Madrid 28040, Spain.
ºNottingham Centre for Geomechanics, University of Nottingham, University Park NG7 2RD Nottinghamshire, UK.
+ Department of Engineering Science, University of Oxford, Parks Road, Oxford, OX1 3PJ, UK.

1 Introduction

Rock-socketed piles are usually employed to support loads from a superstructure and to transfer the loads to stronger and deeper rock layers, with loads being carried by the pile base, shaft, or a combination of both. It is well known (Pells et al. 1978; Seidel and Collingwood 2001) that shaft resistance can be fully mobilized at much lower pile displacements than base resistance, hence understanding the development of shaft resistance is a key aspect in assessing the behavior of rock socketed piles under working loads.

O'Neill et al. (1996) suggested that, in addition to rock strength, there are many parameters that should be considered to evaluate the response of rock-socketed piles, for example (a) the construction method, (b) drilling tools used, (c) the socket roughness, and (d) the embedment ratio (L/D, where L is socket embedment and D is pile diameter). Small-scale load tests conducted by Dai et al. (2017), as well as discrete element modelling results presented by Gutiérrez-Ch et al. (2018, 2019, 2020a), demonstrated that the socket roughness and the normal stiffness at the rock-pile interface are critical factors affecting rock-socketed pile behavior.

Despite previous efforts to estimate the shaft resistance of rock-socketed piles considering socket roughness (Horvath et al. 1983; Seidel and Haberfield 1995; Seidel and Collingwood 2001; Nam and Vipulanandan 2008; Dai et al. 2017; Gutiérrez-Ch et al. 2020a), a more in-depth analysis using load tests is needed. Tests conducted within a geotechnical centrifuge (Leung and Ko 1993) provide some benefits compared with full-scale tests or with tests conducted in the laboratory at 1 g, including (i) the difficulties and costs associated with full-scale tests, (ii) the ability within small-scale experiments to control parameters such as socket roughness and soil/rock properties, and (iii) reproduction of the full-scale stress fields –e.g., stress gradients, and/or the influence of the stress-dependent volumetric response of the rock– that occurs in real applications (that can be reproduced in full-scale tests but not in model tests at 1 *g*). Centrifuge modelling allows the study of geotechnical problems within a small scale model by subjecting the model to increased acceleration fields (i.e. increased levels of gravity, *g*), thereby increasing the self-weight stresses and reproducing the full-scale stress field (Taylor 1995).

Leung and Ko (1993) conducted centrifuge tests of piles socketed in a soft pseudo-rock prepared using a mixture of gypsum cement and water; the intact uniaxial compressive strength of the pseudo rock was σ_c = 2–12 MPa. Leung and Ko's test results suggest that centrifuge testing can reproduce real rock-socketed pile behavior. Dykeman and Valsangkar (1996) carried out centrifuge tests in soft pseudo-rock made from a mixture of sand, cement, bentonite and water (σ_c = 1–12 MPa). They performed axial and lateral loading of caisson foundations made from aluminum, with socket roughness replicated by machining into the outer surface of the model foundation, at a 5 mm spacing, 0.5 mm deep $\times$ 0.5 mm wide circular asperities. Their results indicated that socket roughness increases the load capacity of rock-socketed piles, but they did not measure the distribution of shaft resistance along the piles and provided no insight into the load transfer mechanisms along the (rough) socket shaft. Additional centrifuge tests of large-diameter piles and pile groups socketed into rock were conducted by Zhang and Wong (2007) and Xing et al. (2014); their results further demonstrated the feasibility of centrifuge modelling to reproduce the behavior of rock-socketed piles, although they did not consider socket roughness in their analyses.

This paper aims to address some shortcomings in the previous research. In particular, geotechnical centrifuge tests and fiber Bragg grating strain sensing techniques are used to measure pile settlements and the distribution of pile shaft resistance along the pile-rock interface during axial loading tests of rock-socketed piles with varying degrees of socket roughness. As described below, these advanced experimental techniques provide new insight into the influence of socket roughness on rock-socketed piles, and on their global stiffness and load transfer mechanisms.

2 Centrifuge modelling

The centrifuge tests presented in this paper were conducted at 50 *g* (i.e. 50 times Earth's gravity) using the University of Nottingham Centre for Geomechanics (NCG) 2 m radius, 50 *g*-ton geotechnical centrifuge. According to centrifuge test scaling laws (Taylor 1995), length in a centrifuge model is reduced compared to a full-scale prototype by the gravity scale factor N ($l_m = l_p/N$, where l is length and the subscripts *m* and *p* denote model and prototype, respectively) and force is scaled by N^2 ($F_m = F_p/N^2$, where F is force). Adoption of $N = 50$ in these centrifuge tests allowed replication of a practical range of the geometric socket roughness values, along with reasonable demands for axial pile loads (less than the 10 kN limit of the load actuator used for the centrifuge tests). This section provides a description of the pseudo-rock (used to replicate a soft rock), the model piles and instrumentation, as well as the centrifuge model set-up.

2.1 Pseudo-rock

The effect of socket roughness is particularly significant for piles socketed in soft rocks with an intact uniaxial compressive strength of σ_c = 1–12 MPa (Seidel and Collingwood 2001). To produce rock samples with an intact uniaxial compressive strength σ_c close to 1 MPa, pseudo rock samples were prepared using a mixture of sand, cement, bentonite and water (see **Table 1**). Three cube tests were performed on samples (102 mm) stored and cured in a humid environment after 44-days, with average values of σ_c = 1.14 MPa, Young's modulus of E = 90.6 MPa, and Poisson's ratio of ν = 0.34 (see **Table 2**). Also, considering the above properties, a shear modulus of $G = E/2(1+\nu)$ = 33.8 MPa for the pseudo-rock sample can be derived.

[Table 1 approx. here]

[Table 2 approx. here]

2.2 Model piles

2.2.1 Manufacturing

The model piles were machined from aluminum (Young's modulus E = 69 GPa) tubes with external and internal nominal diameters of 15.87 mm and 11.81 mm, respectively (see **Fig. 1**). At 50 g, the model piles have an axial stiffness (EA; where A is the cross section area) equivalent to a 0.8 m diameter solid concrete pile (Young's modulus E = 30 GPa) at prototype scale. The nominal length of the piles is 80 mm at model scale (4 m at prototype scale).

[Fig. 1 approx. here]

To assess the influence of socket roughness on the response of a pile to axial loading, the model piles were manufactured with different roughness profiles. Previous works have analyzed the influence of roughness using pile-rock interfaces with triangular asperities (Johnston et al. 1987; Kodikara and Johnston 1994; Gu et al. 2003; Xu et al. 2020) or with sinusoidal asperities (Dai et al. 2017). In this research, sinusoidal pile-rock interfaces were used because they provide a reasonable replica of sockets drilled in soft rock with an auger tool (O'Neill et al.,1996; Hassan et al. 1997). However, this is only an approximation, and roughness patterns developed in real rock sockets drilled in the field may be different to those considered herein. The adopted sinusoidal profiles, though not matching exactly with reality, provide the consistency between tests that is required to obtain the desired new insights on the effect of socket roughness on the response of axially loaded rock-socketed piles.

To simulate the roughness profiles, sinusoidal surfaces with asperity amplitudes of 0, 0.2, 0.4, and 0.8 mm at a wavelength of 10 mm (model scale) were used (see **Fig. 1**). These values correspond to asperity amplitudes of 0, 10, 20, and 40 mm and to a wavelength of 500 mm at prototype sale, which are similar to those typically obtained with conventional or special drilling tools (O'Neill et al. 1996; Gutiérrez-Ch et al. 2020a). The four model piles are denoted using their roughness factor (RF), which was defined by Horvath et al. (1983) as $RF = (h_m L_t)/(RL)$, where h_m is the average height of asperities, R is the nominal socket radius, L_t is the total travel distance along the socket wall, and L is the nominal socket length (see **Fig. 1**). The asperity dimensions listed above correspond to values of $L_t = 80$, 80.34, 81.36 and 85.34 mm, and to RF values at model scale of $RF = 0.000$, 0.025, 0.050 and 0.106, respectively (see **Fig. 2**).

[Fig. 2 approx. here]

A literature review by Gutiérrez-Ch et al. (2020a) indicated that sockets drilled with standard tools tend to produce asperities with amplitudes less than or equal to 10 mm (prototype scale), which could be classified as “smooth” piles; however, if the rock is highly fractured or special drilling tools are used, the amplitudes of asperities at the socket could be larger (i.e., more than 10 mm) which would be classified as “rough” piles. Thus the model piles with $RF =$ 0.000, 0.025 would represent “smooth” piles, while the model piles with $RF =$ 0.050, 0.106 would be “rough” piles.

2.2.2 Instrumentation

To record the axial load along the model piles, fiber Bragg grating (FBG) sensors were bonded to the internal surface of the model piles. An FBG sensor is a device that measures the shift in the wavelength of light reflected at a “grating” etched into an optical fiber that is caused by strain or temperature changes (Kreuzer 2006; Kashyap 2010; Alvárez-Botero et al. 2017). Advantages of FBG strain sensors compared with conventional strain gauges that are particularly relevant to centrifuge testing include their insensitivity to electrical noise and their small/lightweight form (Kreuzer 2006; Song et al. 2019; Song 2019). The FBG sensors were particularly advantageous for the tests presented here, since their small size allowed them to be installed inside the model piles (which would not have been possible with conventional foil strain gauges), thereby enabling the accurate manufacturing of the geometric roughness on the outer surface of the piles. An illustration of an FBG strain sensor is presented in **Fig. 3**a. The FBG sensors were made from a single-mode optical fiber, which was etched using an excimer laser. The reflectivity of the FBG sensors is greater than 90%. **Fig. 3**b illustrates the method used to install the optical fibers in the piles: (1) the fiber was inserted into the pile through a hole drilled at an inclined angle near the top of the pile (the pile head assembly shown in **Fig. 1** did not allow for the cable to be passed through its upper end). (2) The end of the fiber near the pile top was bonded to the pile using superglue (Loctite Superglue precision). (3) The fiber was then strained from the other end using a modified micrometer – this ensured the fiber was straight while also facilitating the measurements of tensile and compressive loads. (4) Superglue was then applied along the fiber, followed by a UV cured adhesive to ensure the FBG sensors were fully bonded to the model pile.

The model piles were calibrated on a loading frame (uniaxial compression), and a linear relationship between FBG wavelength shift and the applied load was obtained. For additional details about the calibration conducted, see Gutiérrez-Ch et al. (2020b). Each model pile has two optical fibers, with three FBG sensors per fiber, located on opposite sides of the internal surface of the pile and labelled according to their distance (H) from a reference point at the top of the pile, normalized by the model pile radius (i.e., H/R, see **Fig. 1**a). At a given depth (H/R), the axial force is determined from the two Braggs at that position. Also, note that only three FBG sensors were used because of the difficulty to add more FBGs to the optical fiber (the adopted FBG sensors have a length of 10mm and the pile is 100mm long).

[Fig. 3 approx. here]

2.3 Centrifuge model preparation

Each centrifuge model was prepared as follows. (1) To remove the contribution of pile base resistance, a cylindrical piece of soft polystyrene (with diameter and length equal to the pile diameter) was attached to the bottom of the model piles (see **Fig. 4**a), hence the pile resistance was derived solely from its shaft. (2) The prepared pseudo-rock mixture was poured (in three layers) into 20 cm diameter, 20 cm high steel cylindrical containers, with the container being vibrated on a shake-table after each layer. Boundary effects of these types of experiments are expected to be minimal as long as the "clear distance" from the pile to the edge of the container exceeds four times the pile diameter (Dykeman and Valsangkar 1996; Xing et al. 2014); for these tests, the clear distance was five times the pile diameter. (3) The model piles were pushed into the mixture and set to the designed position using a temporary frame mounted to the top of the steel cylinder (**Fig. 4**b). The container was then vibrated again to ensure adhesion between the pseudo-rock mixture and the model pile, according to the procedure described by Dykeman and Valsangkar (1996) and Dai et al. (2017). (4) The containers were stored and cured under high humidity conditions for 44 days. A typical model pile-pseudo-rock assembly is presented in **Fig. 4**c.

[Fig. 4 approx. here]

In practice, the normal stress applied on the pile-rock interface is zero before the concrete is placed into the socket, and the normal stress acting on the socket sidewalls could increase during placement of concrete (Seidel and Collingwood 2001; Haberfield and Lochaden 2018). This aspect is not considered during the centrifuge model preparation conducted herein; however, a parametric study conducted by Seidel and Collingwood (2001), and the analysis of load test data conducted by Asem (2020), strongly suggest that the initial normal stress at the pile-rock interface does not substantially affect the peak shaft resistance of rock-socketed piles, unless an expansive concrete is used. Therefore, and since expansive concrete was not employed in this work, it is expected that the effect of the initial normal stress acting on the socket sidewalls could be neglected.

2.4 Centrifuge tests

After 44-days of curing, each pseudo-rock container was placed on the centrifuge and steel plates (30 mm thick) were added to the surface to impose a vertical stress of 120 kPa at 50 *g* (replicating 6 m depth of overburden with an average unit weight of 20 kN/m^3) (**Fig. 5**b). The pile loading/measurement system was then installed, comprising of a loading frame, two L03 MecVel ball screw actuators (each with a maximum 5 kN load capacity and 100 mm stroke), a load cell, and a connector (**Fig. 5**). The ball and socket actuator-pile connection, illustrated in **Fig. 5**c, allowed the pile to move separately from the load actuator during centrifuge spin-up, with the pile moving downwards as a result of the self-weight of the pile and associated spacer, load cell, and connector. The model pile settlement was measured using a single linear variable differential transducer (LVDT) positioned on an aluminum plate located above the pile cap (**Fig. 5**b). The load along the model pile was obtained using the FBG sensors and an FBG interrogator located within the centrifuge data acquisition cabinet (see **Fig. 5**a).

For each test, the acceleration of the centrifuge was gradually increased to 50 *g*, at which point the model piles were loaded axially at a displacement controlled rate of 0.1 mm/s. The axial load, displacement, and the wavelength shift of the FBG sensors were recorded at 10 Hz.

[Fig. 5 approx. here]

3 Results

3.1 Preliminary comments

Results are presented at prototype scale relative to readings obtained upon reaching 50 *g*. The head load, the axial load and the shaft resistance mobilized along the pile during the spin-up are not considered, hence results illustrate changes due to pile loading under a constant g-level. Analyses were conducted in this way because (a) the head load mobilized at the end of the spin-up due to the assembly above the piles was only of 0.25 MN (prototype scale) for all models, which is very small when compared to the final pile loading, which reached a minimum of 6.5 MN (i.e., the initial loading after spin-up to 50 *g* was about 3.8% or less of the final load; see **Fig. 6**a); and because (b) during spin-up, the self-weight of the UV adhesive used to attach the FBGs to the piles caused additional FBG readings unrelated to pile loading that are difficult to quantify, leading to some uncertainty of the absolute pile load readings measured by the FBGs during spin-up (note that this does not affect axial load measurements during pile loading after spin-up, since variations of FBG recorded values are analyzed at a constant g-level).

Pile settlement results are presented in dimensionless form (normalized by the pile diameter) to facilitate discussion of results. This adopted normalization convention will not necessarily allow the interface response from these tests to be directly compared to other studies, hence readers should apply appropriate judgement. However, as all tests presented here relate to a consistent pile size and interface type, the adopted convention is satisfactory.

Similarly, some corrections were made to the initial segment of the load-settlement curve of the model pile with $RF = 0.050$, since this pile rotated and moved upwards at the beginning of the tests. The correction involved linearizing the initial curved section of the "raw" load-settlement data, since other curves (for $RF = 0.025$ and $RF = 0.106$) demonstrated such a linear trend upon initial loading (these aspects are discussed further below, and a Supplemental Data file is presented to provide the "raw" data along with an additional discussion of the correction and its implications on subsequent data interpretation.)

3.2 Load-settlement response

The load-displacement curves for the rock-socketed piles with different degrees of socket roughness are shown in **Fig. 6**a. The model pile with $RF = 0.000$ is not presented in **Fig. 6** because it failed during centrifuge spin-up, therefore, its results are not considered in the data analysis since the pile was in a post-peak (failure) state when loading started at 50 g. All piles were loaded until the pile head settlement (δ) exceeded 20% of the pile diameter ($\delta/D >$20%).

[Fig. 6 approx. here]

Experimental results presented in **Fig. 6** demonstrate that socket roughness is a crucial factor affecting rock-socketed pile shaft resistance and the overall stiffness response of the pile. For a pile head settlement equivalent to 1% of the pile diameter ($\delta = 1\%D$), the loads (P) on the pile are 1.18 MN, 1.82 MN, and

4.70 MN, and the global stiffnesses (i.e., P/δ) are 0.15 MN/mm, 0.23 MN/mm and 0.61 MN/mm for model piles with $RF =$ 0.025, $RF =$ 0.050 and $RF =$ 0.106, respectively. Similarly, an influence of socket roughness was also observed in the results of field tests (see **Table 3**) conducted by Horvath et al. (1983) and Seol and Jeong (2007) on full-scale piles socketed in shale and gneiss, respectively, considering shaft resistance only. From **Table 3** it can be noted that, for $\delta = 1\%D$, rougher piles supported a higher working load that is about 1.3 (gneiss) to 1.5 (shale) times higher than for smooth piles.

[Table 3 approx. here]

As can be observed in **Fig. 6**a, the load-settlement curve of the model pile with $RF =$ 0.025 increases linearly to an initial peak value (for $\delta = 0.5\%D$). With further increases in pile settlement, the pile head load decreases, probably representing a loss of the bonding at the pseudo-rock-pile interface. Then, with further displacement (for $\delta > 1\%D$), the pile transfers its axial load to the front of the asperities within the rock, so that its load capacity increases again until a second peak is reached (for $\delta = 19.8\%D$). For rougher piles ($RF =$ 0.050 and $RF =$ 0.106), a bonding failure at the pseudo-rock-pile interface is not observed. The load capacity increases until the maximum load capacity is reached; after this load threshold, the load capacity decreases. Also, results in **Fig. 6**a show that the post-peak shaft resistance – or the shaft's resistance beyond the settlement (δ_{P-peak}) associated with the peak load – tends to be more ductile for rougher piles. This behavior can be explained by the fact that rougher interfaces tend to dilate more and, as a consequence, lead to higher normal stresses at the pile-rock interface that produce higher interface resistances (Pells et al 1978; Gutiérrez-Ch et al. 2021).

Finally, the load-settlement results suggest that there might be an upper roughness limit beyond which, for large settlement levels (say, for $\delta > 10\%D$), the load capacity and the global stiffness no longer increase (i.e. increasing roughness above $RF = 0.050$ did not have a significant effect; see **Fig. 6**). This observation is consistent: (i) with experimental results of Dai et al. (2017), who conducted rock-socketed pile tests with different socket roughness at 1 *g*, but overcomes the interpretation uncertainties of their results, since centrifuge test results account better for the influence of scale and geometry, through the consideration of a more realistic stress field around the pile (Dai et al. 2017 indicate that "there may be scale effects in the[ir] shaft resistance test results" conducted at 1 *g*); and (ii) with numerical results of Gutiérrez-Ch et al. (2020a, 2021) who conducted discrete element method (DEM) load test simulations in piles socketed in sandstone and gneiss with similar RF values.

3.3 Axial load

The distribution of mobilized axial load (change in axial load along the pile) with depth during pile loading was obtained using the measured wavelength shifts of the FBG sensors (see **Fig. 1**). As mentioned earlier, the rock-socketed piles had a polystyrene base; hence the base resistance can be neglected. The results of the mobilized axial load are presented at prototype scale.

Fig. 7 shows the distribution of the mobilized axial load along the pile for several settlement values (including the settlement, δ_{P-peak}, associated with the maximum axial load in **Fig. 6**) for all centrifuge tests conducted. It can be observed (i) that mobilized axial loads along the pile, for a given settlement, decrease with depth; (ii) that mobilized axial loads along the pile increase as the load applied at the pile head increases, until the peak value is reached; and (iii) that mobilized axial loads along the pile decrease after this threshold (i.e., for $\delta > \delta_{P-peak}$), but with smaller, or more ductile, reductions in rougher piles. To our knowledge, this is the first time that the influence of roughness on the axial load distribution of rock-sockets has been measured experimentally (in the field or in the laboratory).

It is important to highlight that, after processing the measurement data for the model pile with $RF = 0.025$, an anomalous distribution of the mobilized axial load with depth was obtained; in particular, the mobilized axial load at 20 mm depth was greater than at 0 mm depth (a "Supplementary Data" file has been provided to discuss details of the measured data and of the uncertainties associated with their interpretation). This trend is unexpected, and may be explained by the fact that, during casting (44 days), the pile could have reacted with the pseudo-rock, causing a change to the relationship between pile/FBG strain and applied load. This is because the pseudo-rock contains cement (alkalis), which can react with aluminum, resulting is some corrosion of the external surface of the piles. After the tests, some corrosion along the pile surface was identified. In such a case, the thickness of the aluminum pile would be less than the pile prior to casting, which would imply an error within the adopted FBG sensor calibration factors (calibrations were conducted for all piles prior to casting; for the pile with $RF = 0.025$, an additional calibration was conducted after the centrifuge test to investigate the anomaly discussed above, see the Supplementary Data). To explore this justification, **Fig. 8** presents the results of the calibration factors obtained before and after the centrifuge test for this pile. (Note that FBG_1 is not shown in the post-test results of **Fig. 8** because the sensor did not respond during the post-test calibration). As can be observed in **Fig. 8**, a variation of the calibration factors was found, potentially explaining why the mobilized average axial loads recorded by the FBG sensors located at $H/R = 2.5$ and $H/R = 5$ ($FBG_{3\text{-}6}$ and $FBG_{2\text{-}5}$, respectively, see **Fig. 1**) are greater than the pile head load recorded by the load cell. Therefore, results presented in **Fig. 7**a (and in the following sections) correspond to values obtained with post-test calibration factors for the pile with $RF = 0.025$, while for piles with $RF = 0.050$ and $RF = 0.106$, the pre-test calibration factors have been employed. (See the Supplementary Data for additional details about the uncertainties relating to the variation of the calibration factors and their impact on the mobilized axial loads.)

[Fig. 7 approx. here]

[Fig. 8 approx. here]

3.4 Shaft resistance

The distribution with depth of the (locally) mobilized average shaft resistance (i.e., of changes of average shaft resistance upon pile loading after spin-up to a constant 50 g-level, $f_{ave,l}$), for a given pile head settlement, can be obtained from the difference of the mobilized axial load between two consecutive reference points at which pile axial loads have been measured, as:

$$f_{ave,l} = \frac{F_{i,\delta} - F_{i+1,\delta}}{\pi D L_{i \to i+1}} \tag{2}$$

where $F_{i,\delta}$ and $F_{i+1,\delta}$ are the mobilized axial loads (i.e., change in axial loads upon loading under constant g-level) at two consecutive reference points (e.g., at the pile FBG sensors located at $H/R = 2.5$ and $H/R = 5$, see **Fig. 1** for FBG reference i), D is the pile diameter, and $L_{i\to i+1}$ is the nominal length between the two consecutive reference points (i.e., from location i to $i+1$). Hence the $f_{ave,l}$ computed using Eq. 2 is considered constant from location i to $i+1$. In addition, since D and $L_{i\to i+1}$ are nominal values which are equal for all piles, the shaft area in Eq. (2) is assumed to be the same for all the piles.

The distribution of $f_{ave,l}$ (with depth) for a given pile head settlement is shown in **Fig. 9**. The peak value curves represent the value of $f_{ave,l}$ computed for a pile head settlement associated with the maximum mobilized axial load from **Fig. 6** (i.e., for $\delta = \delta_{P-peak}$). Results show that $f_{ave,l}$ distributions with depth, for a pile head settlement of $1\%D$, are similar for rougher piles (i.e., with $RF = 0.050$ and $RF = 0.106$), so that the mobilized average shaft resistance is greater at the pile head (from $H/R = 0$ to $H/R = 2.5$) than at the pile toe; while for the smoother pile (i.e., with $RF = 0.025$) the distribution with depth tends to be more homogenous.

[Fig. 9 approx. here]

Also, **Fig. 9** shows that, as the applied load increases and the maximum mobilized axial load is reached, $f_{ave,l}$ starts to decrease in the upper portion of the pile (from $H/R = 0$ to $H/R = 2.5$), and therefore to increase in the lower portion of the pile (from $H/R = 5$ to $H/R = 10.1$). To illustrate this, **Fig. 10** shows the mobilized average shaft resistance recorded at different depths below the socket (from $H/R = 0$ to $H/R = 10.1$), for $0.5\%D \leq \delta \leq 8\%D$. Once the pile head settlement for the model pile with $RF = 0.106$ goes beyond $\delta > 1\%D$, $f_{ave,l}$ tends to increase more in the lower region of the pile than in the region near its head; a similar behavior is noted when $\delta > 4\%D$ for the model pile with $RF = 0.050$, see **Fig. 10**. This trend, which is clearer for rougher piles ($RF = 0.050$ and $RF = 0.106$, see **Fig. 9**b-c) than for the smoother pile ($RF = 0.025$, see **Fig. 9**a), can be explained by the roughness at the pile-rock interface, since $f_{ave,l}$ is fully mobilized first near the pile head.

[Fig. 10 approx. here]

This behavior is also clearly observed when one analyses how the mobilized average shaft resistance develops with settlement at different portions of the model pile (see **Fig. 11**). For example, **Fig. 11**c shows such an evolution for the model pile with $RF = 0.106$: it can be observed that the peak value of $f_{ave,l}$ is reached first (i.e. for pile settlements approximately $1\%D$) in the upper region of the pile (from $H/R = 0$ to $H/R = 2.5$), after which it decreases for larger pile settlements. (Note that a similar trend is observed for the piles with $RF = 0.050$ and 0.025, but for higher pile head settlements; see **Fig. 11**a). This behavior might be due to the fact that, during the initial loading stages, much of the load is transmitted to the front part of the asperities (see **Fig. 11**d) located in the upper region of the pile; then, upon further loading of the pile (or with settlements greater than $1\%D$), degradation and breakage of asperities occur, and the maximum values of average shaft resistance shift downwards (towards the pile toe) where, with further loading, a similar behavior is observed. The reader should note that these settlements are much higher than those associated with standard design methods for piles at working loads (e.g., $\delta = 1\%D$, Whitaker and Cooke 1966). Also, note that failure mechanisms or strain localizations at the pile-interface cannot be shown, since it was generally not possible to extract the piles (or to excavate the rock) after the centrifuge tests without altering the pile-rock interfaces.

These results are in agreement with Gutiérrez-Ch (2020), where a similar load-transfer behavior was obtained from DEM simulations of rock-socketed piles. Also, results are consistent with the trends reported by Pells et al. (1980) based on their field tests with small diameter piles, and with the load-transfer behavior of rough rock-socketed piles inferred by Hassan and O'Neill (1997) from the results of their finite element numerical models. However, such aspects of the load transfer mechanisms of rock-socketed piles had not been previously measured on pile shafts with such a wide range of roughness values.

[Fig. 11 approx. here]

Fig. 12 shows the mobilized average shaft resistance (f_{ave}) – computed as an average of the locally mobilized average shaft resistance along the pile, instead of dividing the pile head load by the nominal shaft area –, as a function of pile head settlement, for all centrifuge tests. Note that, as it should be, the curves in **Fig. 12** are similar to those of pile head load in **Fig. 6**, demonstrating good agreement between the load cell and FBG sensor measurements. Again, as reported in Section 3.2, **Fig. 12** shows that socket roughness greatly affects the average shaft resistance of rock-socketed piles: e.g., for $\delta = 5\%D$, f_{ave} of the pile with $RF = 0.106$ is about 3 times greater than that obtained for the pile with $RF = 0.025$.

These experimental results are qualitatively consistent with the field test results of Seol and Jong (2007) and with the numerical results of Gutiérrez-Ch et al. (2020a), who reported that rougher piles mobilized more f_{ave} than smooth ones. For instance, for piles socketed in sandstone and for $\delta = 1\%D$, Gutiérrez-Ch et al. (2020a) reported that the average shaft resistance for a pile with $RF = 0.106$ is around 4.2 times higher than the f_{ave} of a pile with $RF = 0.025$ (see **Table 3**). Similarly, it has also been noted (by Seol and Jong (2007) for piles socketed in gneiss and by Dykeman and Valsangkar (1996) in pseudo-rock) that rough piles mobilized 1.3 to 1.6 times more f_{ave} than smooth piles, for $\delta = 1\%D$ (see **Table 3**). This behavior might be due to effects of the higher dilation associated with rough piles, which increases the normal stress at rough pile-rock interfaces (i.e. with higher RF).

Experimental results also showed a quasi-linear (elastic) behavior for δ values of less than about $1\%D$, which was defined by Asam and Gardoni (2019) as initial shear stiffness (K_{si}) (see **Fig. 12**), after which plastic behavior is observed. This finding is particularly significant in practice, since a maximum pile head settlement of 1%*D* is often considered for design under working loads (see e.g., Whitaker and Cooke 1966). It also experimentally supports the results of Gutiérrez-Ch et al. (2019, 2020a) who, based on micro-crack propagation from numerical results using the DEM, suggested that the $1\%D$ settlement threshold is suitable to avoid excessive damage of rock-concrete interfaces of rock-socketed piles.

[Fig. 12 approx. here]

3.5 Comparison with design methods

Usually, the shaft resistance of rock-socketed piles is estimated using empirical criteria that are a function of the uniaxial compressive strength of the weaker material at the socket interface (intact rock or concrete pile). Their formulation can be typically generalized as:

$$f_{ave,peak}[\mathrm{MPa}] = \alpha\sigma_c[\mathrm{MPa}]^{\beta} \tag{3}$$

where $f_{ave,peak}$ is the average ultimate shaft resistance, and α and β are empirical factors specific to each criterion (for a recent compilation of α and β values, see Gutiérrez-Ch et al. 2020a). However, the wide variability of α and β suggests that, in agreement with the conclusions of O'Neill et al. (1996) after their analysis and interpretation of 245 load tests in different types of materials, other parameters in addition to σ_c are required for an improved estimation of $f_{ave,peak}$.

This section compares the results of some common empirical formulations with the results measured in the centrifuge tests conducted in this research. As mentioned earlier, the average shaft resistance mobilized during spin-up has been neglected (the error introduced when compared to the f_{ave} values reported in **Fig. 12** is very small, i.e., 3.8% or less). This value is well below the uncertainty levels and safety factors associated with typical designs of rock-socketed piles; therefore, the comparison of centrifuge results and empirical formulations can be considered appropriate. The formulations with which results are compared are those of (i) Horvath et al. (1983) using $f_{ave,peak}/\sigma_c = 0.8(RF)^{0.45}$; (ii) O'Neill and Reese (1999), Canadian Foundation Engineering Manual (2006) and AASHTO (2008), which proposed equations to compute $f_{ave,peak}$ based on conservative lower values suggested by Horvath et al. (1983) and by Rowe and Armitage

(1987), with $\beta = 0.5$ and α varying between 0.2 and 0.6, depending on socket roughness ($\alpha = 0.2$ for smooth socket, $\alpha = 0.3$ for rough socket, and $\alpha = 0.6$ for very rough socket with h_m >10 mm); (iii) Seidel and Collingwood (2001) who, based on data from 162 load tests from around the world in a variety of rock types – including shale, mudstone, sandstone, chalk, limestone and schist – proposed the non-dimensional shaft resistance coefficient (SRC), which considers the effect of construction method (η_c), the ratio of rock mass modulus to the UCS ($n = E_m/\sigma_C$), the Poisson's ratio, the average height of asperities, and the socket diameter, which can be used to estimate $f_{ave,peak}$ (for details, see Seidel and Collingwood 2001); and (iv) Salgado (2008), who proposed equations similar to Equation (3), while limiting $f_{ave,peak}$ to 5% of the UCS of the rock or of the concrete with which the pile was constructed. In addition, results are compared with other formulations that do not consider socket roughness, such as those of (v) Rezazadeh and Eslami (2017), (vi) Williams et al (1980) and (viii) Horvath and Kenney (1979). Comparisons are conducted using centrifuge results for f_{ave} associated with a settlement of $\delta = 1\%D$, since the above-mentioned methods were also proposed for this reference pile settlement. Results are illustrated in **Fig. 13**, which shows that the centrifuge measurements obtained provide f_{ave} values that are similar to those obtained with empirical criteria, although there are of course differences among methods. Note also that, for the piles with $RF = 0.025$ and 0.050, most empirical formulations that consider roughness tend to provide values slightly above the centrifuge test measurements; whereas for the pile with $RF = 0.106$, measured values tend to be slightly below the predictions. (For Seidel and Collingwood's (2001) method, only results for $RF = 0.025$ and $RF = 0.050$ are presented; this is because the other RF values considered herein fall outside the roughness ranges for which the method can provide predictions.) Within the formulations that consider socket roughness, those by O'Neill and Reese (1999), Canadian Foundation Engineering Manual (2006) and AASHTO (2008) provide the best agreement with centrifuge measurements for model piles with $RF \geq$ 0.025. A similar trend is observed for predictions obtained with Salgado´s (2008) method, although predictions act, in this case, as an "upper bound" to measurements. Additional measurements would be required to be able to assess the predictive capabilities of these methods with a higher degree of confidence.

[Fig. 13 approx. here]

4 Conclusions

The shaft resistance of rock-socketed piles is usually estimated based on the uniaxial compressive strength of the weaker material at the socket interface (intact rock or concrete pile). However, there are other factors (e.g., the construction method and the drilling tools used, the socket roughness, etc.) affecting the shaft resistance behavior of rock-socketed piles that are not commonly considered but which could significantly influence the strength and load-settlement response of piles socketed into rock. This work extends previous efforts to incorporate the influence of socket roughness into predictions of the shaft resistance of rock-socketed piles.

This paper used centrifuge tests conducted at 50 *g* to analyze the shaft resistance behavior of aluminum piles with different degrees of roughness that are socketed into a soft pseudo-rock with a uniaxial compressive strength in the order of 1–1.15 MPa. The piles were instrumented with fiber Bragg grating (FBG) sensors to measure the load distribution along the pile shaft, hence making it possible to compute the distribution of mobilized average shaft resistance on the piles, as a function of the external loads applied and of the pile settlements. This paper further demonstrates that such centrifuge tests are an economic and appropriate tool to study the behavior of rock-socketed piles under axial loads. In particular, results show that centrifuge tests conducted with FBG sensors are suitable to reproduce the load-settlement response of rock-socketed piles, hence being able to evaluate the effect of socket roughness on shaft resistance of rock-socketed piles. There were, as is often the case with complex experimental studies, some uncertainties in the obtained measurements; these were detailed in the supplementary data along with a discussion on potential implications on obtained outcomes. The experimental uncertainities are considered to be no more significant than typical levels of uncertainty for piling projects.

The centrifuge tests conducted with FBG sensors have also provided experimental evidence and confirmation of important aspects of the load-transfer mechanism of rock-socketed piles; in particular, (i) that rougher piles are more resistant, stiffer, and more ductile than smooth piles; (ii) that, particularly for rougher piles, the upper part of the pile tends to attract more load initially, and that such loads tend to “move downwards” as the pile head load continues increasing; (iii) that the load distribution along the pile is more homogenous in smoother piles than in rougher ones, (iv) that little damage seems to occur at the rock-pile interface for pile head settlements of less than about $1\%D$, given the observation that the load increases linearly with settlement within that settlement range, and (v) that there might be an upper roughness limit above which the load capacity and the global stiffness of the rock-socketed pile stops increasing (for large pile head settlements of, say, more than $10\%D$). Finally, average shaft resistances measured in the centrifuge tests were compared with those predicted with several common formulations from the literature. Centrifuge results tend to agree with the overall trend, although there are of course differences between formulations; additional measurements would be required to assess the predictive capabilities of these methods with more confidence.

5 Data Availability Statement

Some or all data, models, or code that support the findings of this study are available from the corresponding author upon reasonable request (centrifuge test results).

6 Acknowledgements

This research was funded, in part, by the Spanish Ministries of Economy, Industry and Competitiveness and Science and Innovation, under Projects BIA 2015-69152-R and PID2019-108060RB-I00. The first author was the recipient during 2019 of one Fellowship for PhD research provided by the José Entrecanales Ibarra Foundation. The support of both institutions is gratefully acknowledged.

7 Appendix A. Supplementary Data

Supplementary data to this work can be found at:

8 References

AASHTO (American Association of State Highway and Transportation Officials). (2008). “LRFD bridge design specifications.” Washington, DC.

Álvarez-Botero, G., Barón, F.E., Canom C. C., Sosa, O., and Varón, M (2017). “Optical sensing using fiber Bragg gratings: Fundamentals and Applications.” *IEEE Instrum. Meas. Mag.*, 20(2), 33–38. https://doi.org/10.1109/MIM.2017.7919131.

Asem, P. (2020). “The effect of expansive concrete on the side resistance of sockets in weak rock”. Soils Found., 60(1): 274–282. https://doi.org/10.1016/j.sandf.2020.02.002.

Asem, P., and Gardoni, P. (2019). “A load-transfer function for the side resistance of drilled shafts in soft rock”. *Soils Found.,* 59(5), 1241–1259. https://doi.org/10.1016/j.sandf.2019.04.006.

Canadian Geotechnical Society. (2006). *Canadian Foundation Engineering Manual.* 4th edition. Canadian Geotechnical Society. Calgary, Canada.

Dai, G., Salgado, R., Gong, W., and Zhu, M. (2017). “The effect of sidewall roughness on the shaft resistance of rock-socketed piles.” *Acta Geotech.,* 12(2), 429–440. https://doi.org/10.1007/s11440-016-0470-8.

Dykeman, P., and Valsangkar, A. L. (1996). “Model studies of socketed caisson in soft rock.” *Can. Geotech. J.,* 33(5), 747–759. https://doi.org/10.1139/t96-100-321.

Gu, X. F., Seidel, J. P., and Haberfield, C. M. (2003). “Direct shear test of sandstone-concrete joints.” *Int. J. Geomech.,* 3, 21–33. https://doi.org/10.1061/(ASCE)1532-3641(2003)3:1(21).

Gutiérrez-Ch J. G. (2020). “Análisis del Efecto de la Rugosidad en el Contacto Roca-Pilote sobre la Resistencia por Fuste de Pilotes”. PhD Thesis (In Spanish). Universidad Politécnica de Madrid. Spain. https://doi.org/10.20868/UPM.thesis.63589.

Gutiérrez-Ch, J. G., Senent, S., Melentijevic, S., and Jimenez, R. (2021). “A DEM-Based factor to design rock-socketed piles considering socket roughness”. *Rock Mech. Rock Eng*. https://doi.org/10.1007/s00603-020-02347-1.

Gutiérrez-Ch, J. G., Melentijevic, S., Senent, S., and Jimenez, R. (2020a). “Distinct element method simulations of rock-socketed piles: estimation of shaft resistance considering socket roughness.” *J. Geotech. Geoenviron. Eng.*, 146(12): 04020133. https://doi.org/10.1061/(ASCE)GT.1943-5606.0002394.

Gutiérrez-Ch, J. G., Song, G., Heron, C., Marschall, A., and Jimenez, R., (2020b). “Centrifuge modelling of shaft resistance of a rock-socketed pile. Proc., 4th European Conference on Physical Modelling in Geotechnics-ECPMG, 06–08 September, Lulea, Sweden.

Gutiérrez-Ch, J. G., Melentijevic, S., Senent, S., and Jimenez, R. (2019). “DEM models to predict shaft resistance of rock-socketed piles considering socket roughness”. *53rd U.S. Rock Mech./Geomech. Symp.,* 23–26 June: ARMA 19–1757. New York City, New York.

Gutiérrez-Ch, J. G., Senent, S., Melentijevic, S., and Jimenez, R. (2018). “Distinct element method simulations of rock-concrete interfaces under different boundary conditions." *Eng. Geol.*, 240, 123–139. https://doi.org/10.1016/j.enggeo.2018.04.017.

Haberfield, C. M., Lochaden, A. L. E. (2019). "Analysis and design of axially loaded piles in rock". *J. Rock Mech. Geotech. Eng.,* 11(3): 535–548. https://doi.org/10.1016/j.jrmge.2018.10.001.

Hassan, K. M., O'Neill, M. W., Sheikh, S. A., and Ealy, C. D. (1997) "Design method for drilled shafts in soft argillaceous rock." *J. Geotech. Geoenviron. Eng.,* 123(3), 272–280. https://doi.org/10.1061/(ASCE)1090-0241(1997)123:3(272).

Horvath, R. G., and Kenney, T. C. (1979). "Shaft resistance of rock-socketed drilled piers." *Proc., Symp., on Deep Found.,* ASCE, 182-214. Atlanta, USA.

Horvath, R. G., Kenney, T. C., and Kozicki, P. (1983). "Methods for improving the performance of drilled piers in weak rock." *Can. Geotech. J.,* 20(4), 758–772. https://doi.org/10.1139/t83-081.

Johnston, I. W., Lam, T. S. K., Williams, A. F. (1987). "Constant normal stiffness direct shear testing for socketed pile design in weak rock". *Géotechnique*, 37(1), 83–89. https://doi.org/10.1680/geot.1987.37.1.83.

Kashyap, R. (2010). "Fiber Bragg gratings." 2nd Edition, Academic Press.

Kodikara, J. K., Johnston, I. W. (1994). "Shear behavior of irregular triangular rock-concrete joints". *Int. J. Rock. Mech. Min. Sci. Geomech. Abstr.,* 31: 313–322. https://doi.org/10.1016/0148-9062(94)90900-8.

Kreuzer M. (2006). "Strain measurement with fiber Bragg grating sensors." HBM: Darmstadt, Germany.

Leung, C. F., and Ko, H-Y. (1993). "Centrifuge model study of piles socketed in soft rock." *Japanese Soc. Soil Mech. Found. Eng.,* 33(33), 88–91. https://doi.org/10.3208/sandf1972.33.3_80.

Nam, M. S., and Vipulanandan, C. (2008). "Roughness and unit side resistances of drilled shafts socketed in clay shale and limestone". *J. Geotech. Geoenviron. Eng.*, 134(9), 1272–1279. https://doi.org/10.1061/(ASCE)1090-0241(2008)134:9(1272).

O'Neill, M. W., Townsend, F. C., Hassan, K. M., Buller, A., and Chan, P. S. (1996). "Load transfer for drilled shafts in intermediate geomaterials." U.S. Department of Transportation, FHWA-RD- 95–172, Final Report.

O'Neill, M. W., and Reese, L. C. (1999). "Drilled shafts: construction procedures and design methods." FHWA-IF-99-025, Federal Highway Administration, U.S. Department of Transportation, Washington, DC.

Pells, P. J. N., Douglas, D. J., Rodway, B., Thorne, C. P., and McMahon, B. R. (1978). "Design loadings for shales and sandstones in the Sydney region." *Austral. Geomechs.*, G8, 31–39.

Rezazadeh, S., and Eslami, A. (2017). “Empirical methods for determining shaft bearing capacity of semi-deep foundations socketed in rocks.” *Int. J. Rock Mech. Geotech. Eng.,* 9(6), 1140–1151. https://doi.org/10.1016/j.jrmge.2017.06.003.

Rowe, R. K., and Armitage, H. H. (1987). “A design method for drilled piers in soft rock.” *Can. Geotech. J.,* 24(1), 126–142. https://doi.org/10.1139/t87-011.ç

Salgado, R. (2008) “The engineering of foundations”. The McGraw-Hill Companies Inc, New York.

Seidel, J. P., and Collingwood, B. (2001). “A new socket roughness factor for prediction of rock socket shaft resistance.” *Can. Geotech. J.,* 38(1), 138–153. https://doi.org/10.1139/t00-083.

Seidel, J. P., and Haberfield, C. M. (1995). “The axial capacity of pile sockets in rocks and hard soils”. *Ground Eng.,* 28(2), 33–38.

Seol, H. I., Jeong, S. S. (2007). “Shaft resistance characteristics of rock-socketed drilled shafts based on pile load tests.” *J. Korean Geotech. Soc.,* 23(9), 51–63.

Song, G., Marshall, A. M., and Heron, C. M. (2019). “Load redistribution of piles affected by tunnelling: hybrid centrifuge tests using fibre Bragg grating”. *Proc. XVII European Conference on Soil Mech. Geotech. Eng.* Reykjavik, Iceland. https://doi.org/10.32075/17ECSMGE-2019-0236.

Song, G. (2019). “The use of protective structures to reduce tunnelling induced damage to buildings”. Ph.D. Thesis, Faculty of Engineering, University of Nottingham, UK.

Taylor, R. N. (1995). “Geotechnical centrifuge technology.” London: Blackie Academic & Professional.

Whitaker, T., and Cooke, R. W. (1966). “An investigation of the shaft and base resistances of large bored piles in London Clay”. *Proc. Symp. of Large Bored Piles,* 7-49. London, UK.

Williams, A. F., Johnston, I. W., and Donald, I. B. (1980). “The design of socketed piles in weak rock.” *Proc., Int. Conf. Struct. Found. Rock,* 1, 327–347. Sydney, Australia.

Xing, H., Zhang, Z., Meng, M., Luo, Y., and Ye, G. (2014). “Centrifuge tests of superlarge-diameter rock-socketed piles and their bearing characteristics.” *J. Bridge Eng.,* 19(6), 04014010. https://doi.org/10.1061/(ASCE)BE.1943-5592.0000582.

Xu, J., Haque, A., Gong, W., Gamage, R. P., Dai, G., Zhang, Q., and Xu, F. (2020). “Experimental study on the bearing mechanisms of rock-socketed piles in soft rock based on micro X-ray CT analysis”. *Rock Mech. Rock Eng.,* 53: 3395–3416. https://doi.org/10.1007/s00603-020-02121-3.

Zhang, L. M., and Wong, E. Y. (2007). “Centrifuge modelling of large-diameter bored pile groups with defects.” *J. Geotech. Geoenviron. Eng.,* 133(9), 1091–1101. https://doi.org/10.1061/(ASCE)1090-0241(2007)133:9(1091).

List of Tables

Table 1. Mix proportions by percent mass.

Mix proportions by percent mass (%)			
Sand (0.16-mm ≤ Grain size ≤ 1-mm)	Cement (CEM II/A-LL 32.5R)	Bentonite (Sodium)	Water
52.3	12.2	6.5	29.0

Table 2. Results of UCS tests conducted with samples at 44-days age.

	UCS Tests conducted		
	Sample 1	Sample 2	Sample 3
σ_c (MPa)	1.14	1.15	1.12
E (MPa)	85.7	84.4	101.8
ν	0.27	0.32	0.43

Table 3. Axial load and mobilized average shaft resistance supported by rock-socketed piles with different roughness for a pile head settlement of 1% of pile diameter.

Test	Pile	D (m)	L (m)	Type of Rock	σ_c (MPa)	Roughness Description	P (MN)	f_{ave} (MPa)	Reference
Centrifuge tests*	-	0.80	4.00	Pseudo-rock	1.14	$RF = 0.025$	1.18	0.143	This work*
	-					$RF = 0.050$	1.82	0.177	
	-					$RF = 0.106$	4.70	0.467	
Field tests	P1	0.71	1.37	Shale	5.40	$RF = 0.036$	3.10	1.01	Horvath et al. (1983)
	P6				5.60	$RF = 0.100$	4.75	1.55	
Centrifuge* tests	P1	1.00	2.54	Pseudo-rock	1.51	Smooth	3.76	0.47	Dykeman and Valsangkar (1996)
	PR2					Rough	6.00	0.75	
Field tests	MLSU	0.40	1.00	Gneiss	50	Smooth	0.94	0.75	Seol and Jeong (2007)
	MLRU					Rough	1.24	0.99	
Numerical simulations	3	0.80	0.80	Sandstone	21.65	$RF = 0.025$	0.31	1.22	Gutiérrez-Ch et al. (2020a)
	6					$RF = 0.106$	1.42	5.10	

*values at prototype scale

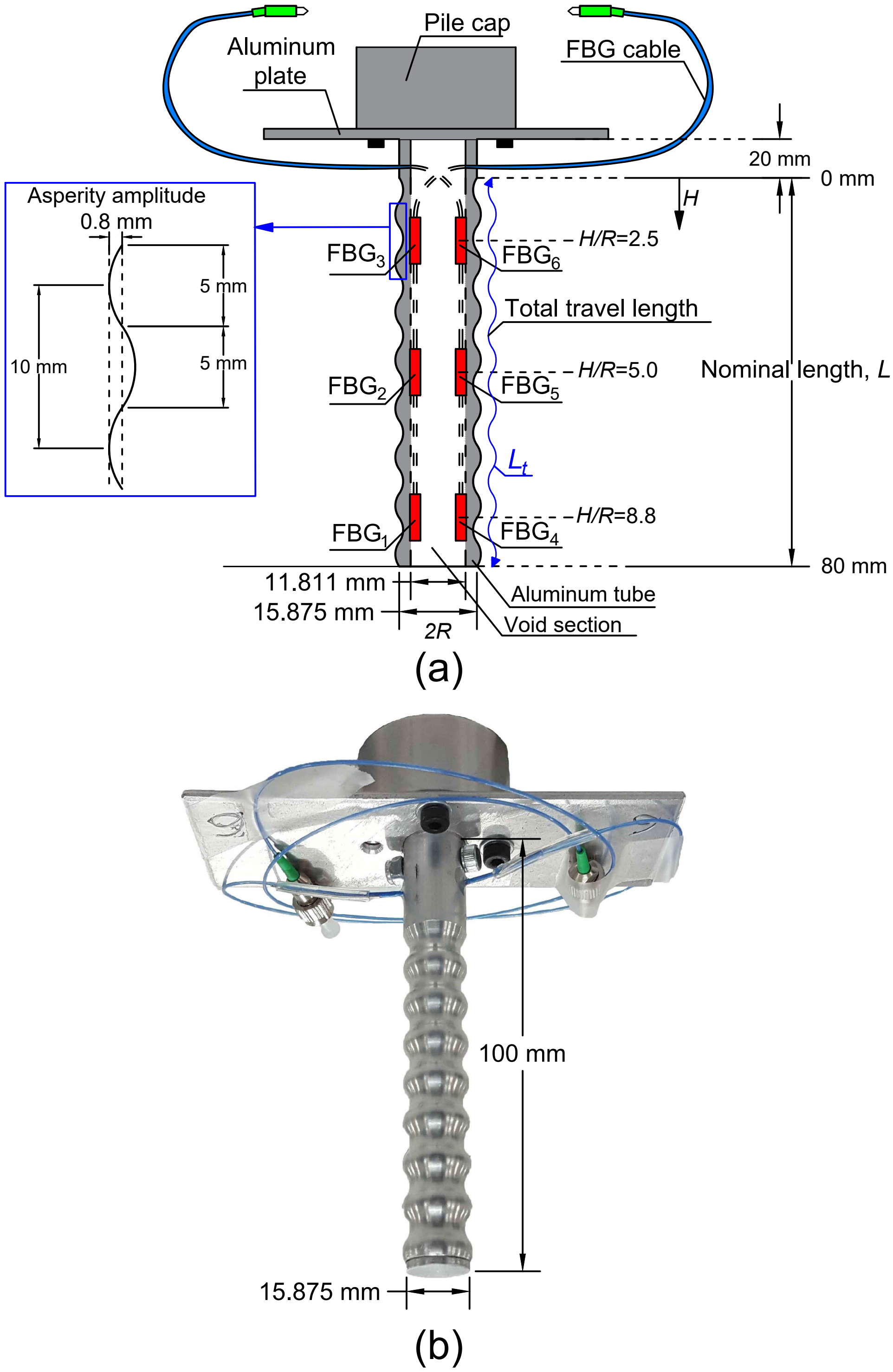

Fig. 1. Aluminum model pile: (a) schematic illustration of the geometric and instrumentation details (b) model pile with RF=0.106 with instrumentation.

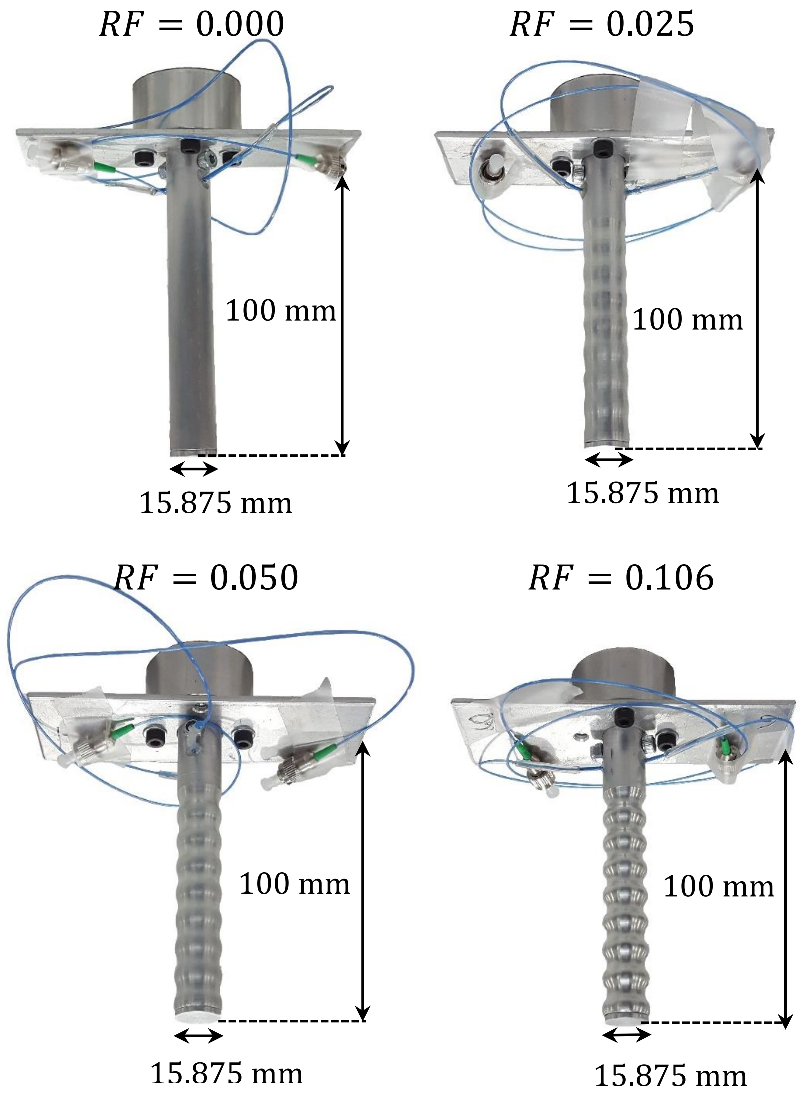

Fig. 2. Model piles with different roughness factor (RF).

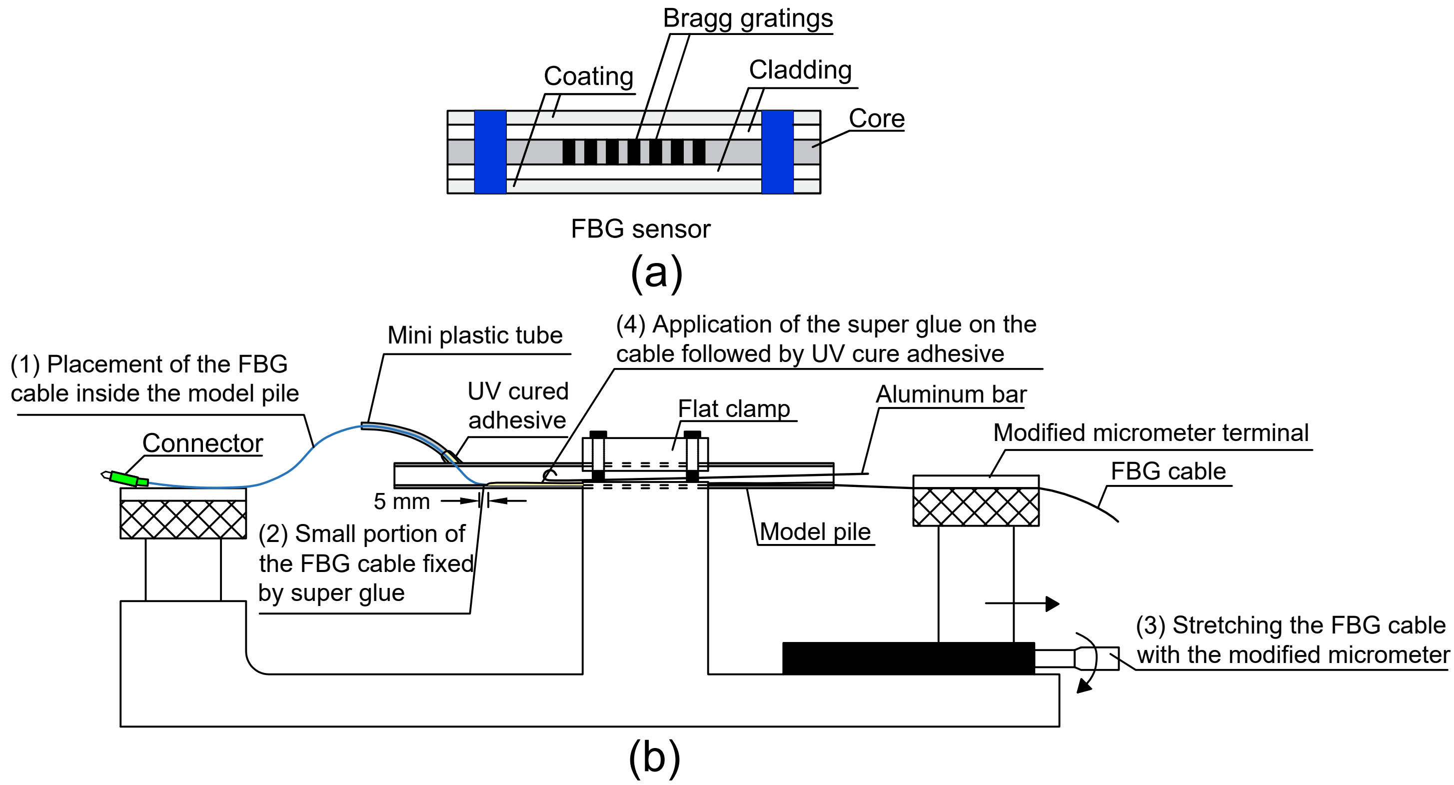

Fig. 3. (a) Detail of the structure of an FBG sensor, and (b) schematic illustration of the installation of an FBG sensor in a model pile.

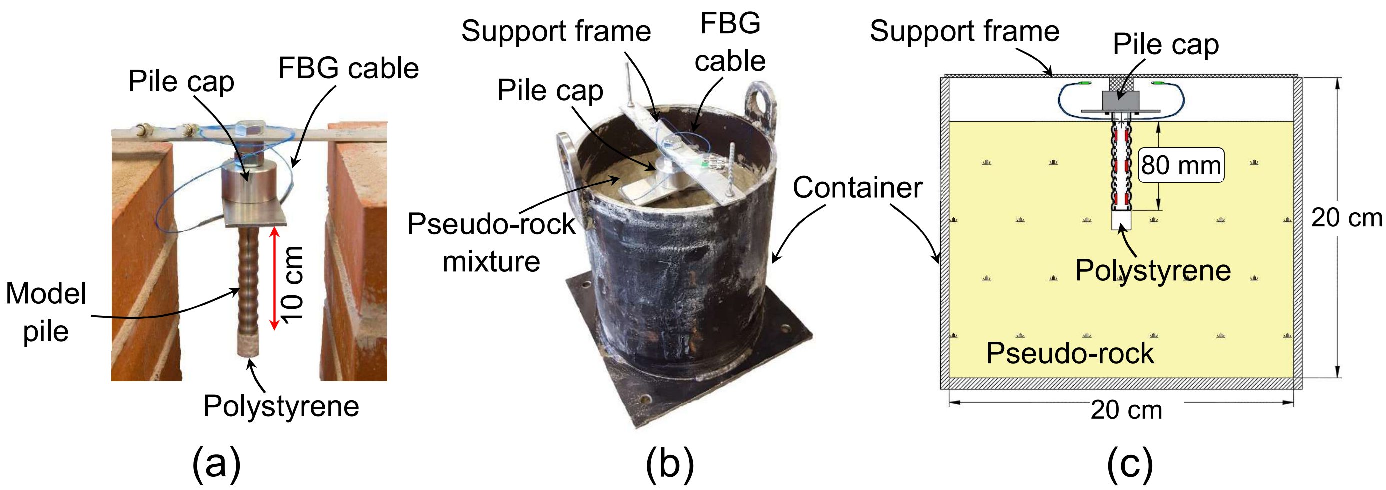

Fig. 4. (a) Model pile ($RF = 0.106$) with polystyrene piece glued to base, (b) steel cylinder container containing pseudo rock, model pile, and temporary frame to hold pile in place, and (c) typical model pile-pseudo-rock assembly.

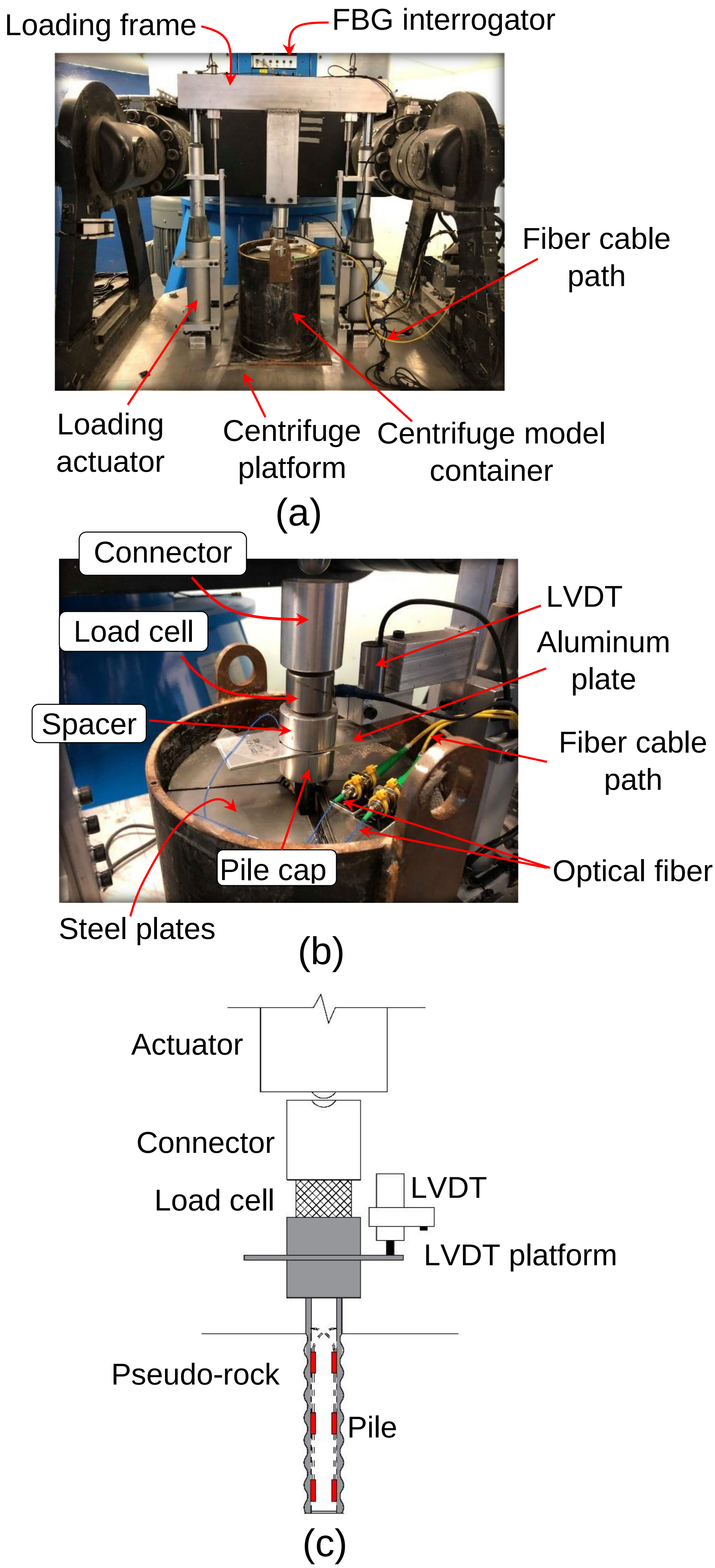

Fig. 5. Centrifuge test set-up: (a) general arrangement of the sample container and loading frame, (b) close-up view of the top of the container, and (c) schematic view of actuator-pile connection.

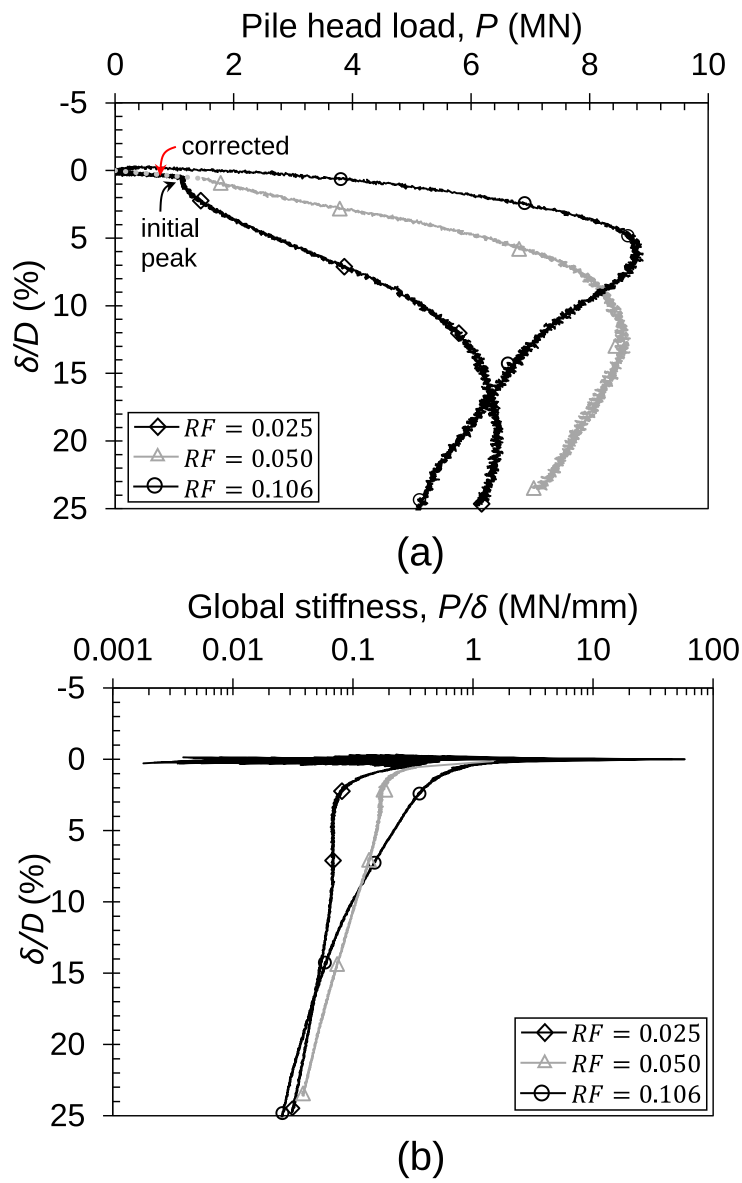

Fig. 6. (a) Pile head load-settlement and (b) global stiffness-settlement curves of centrifuge tests of rock-socketed piles and different roughness profiles.

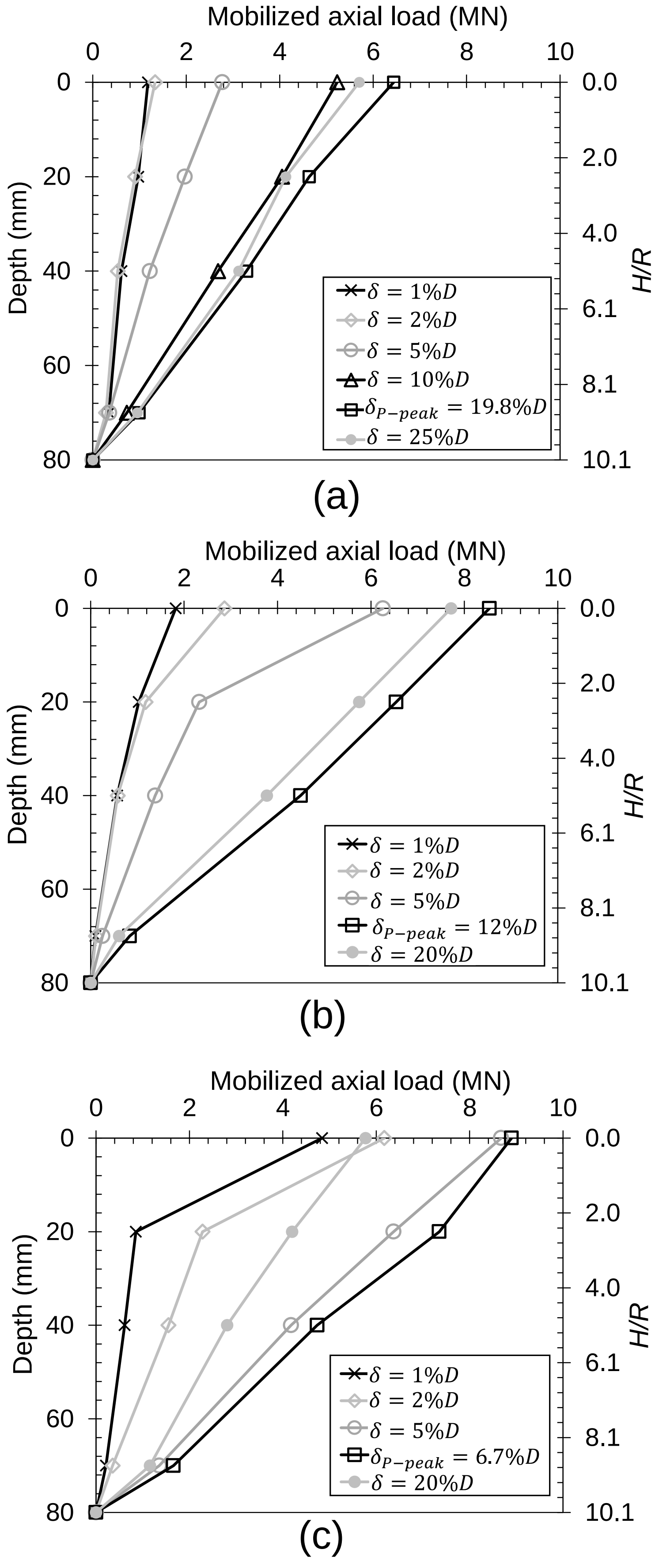

Fig. 7. Mobilized axial load distribution (vs depth) for a given settlement for centrifuge tests with different roughness profiles: (a) RF= 0.025, (b) RF= 0.050, (c) RF= 0.106

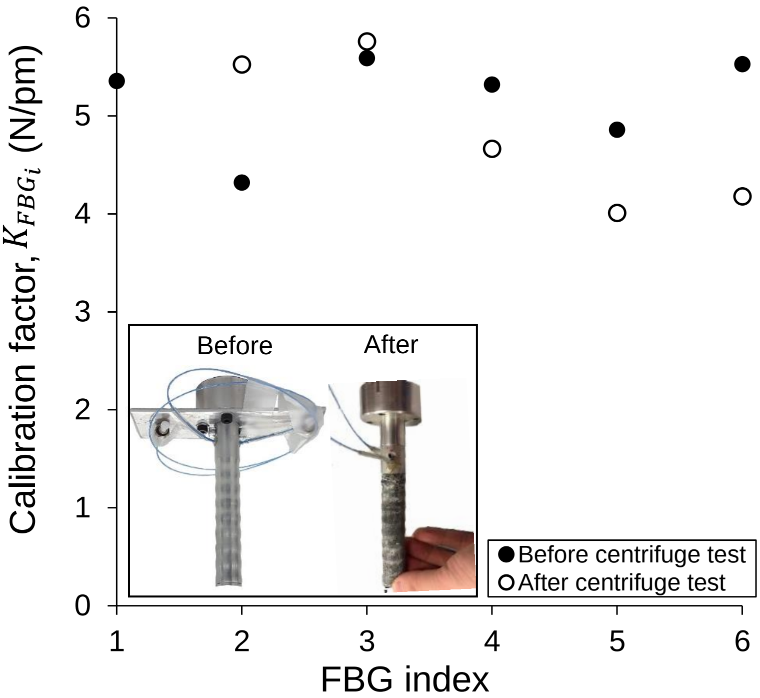

Fig. 8. Variation of the calibration factors for $RF = 0.025$ pile.

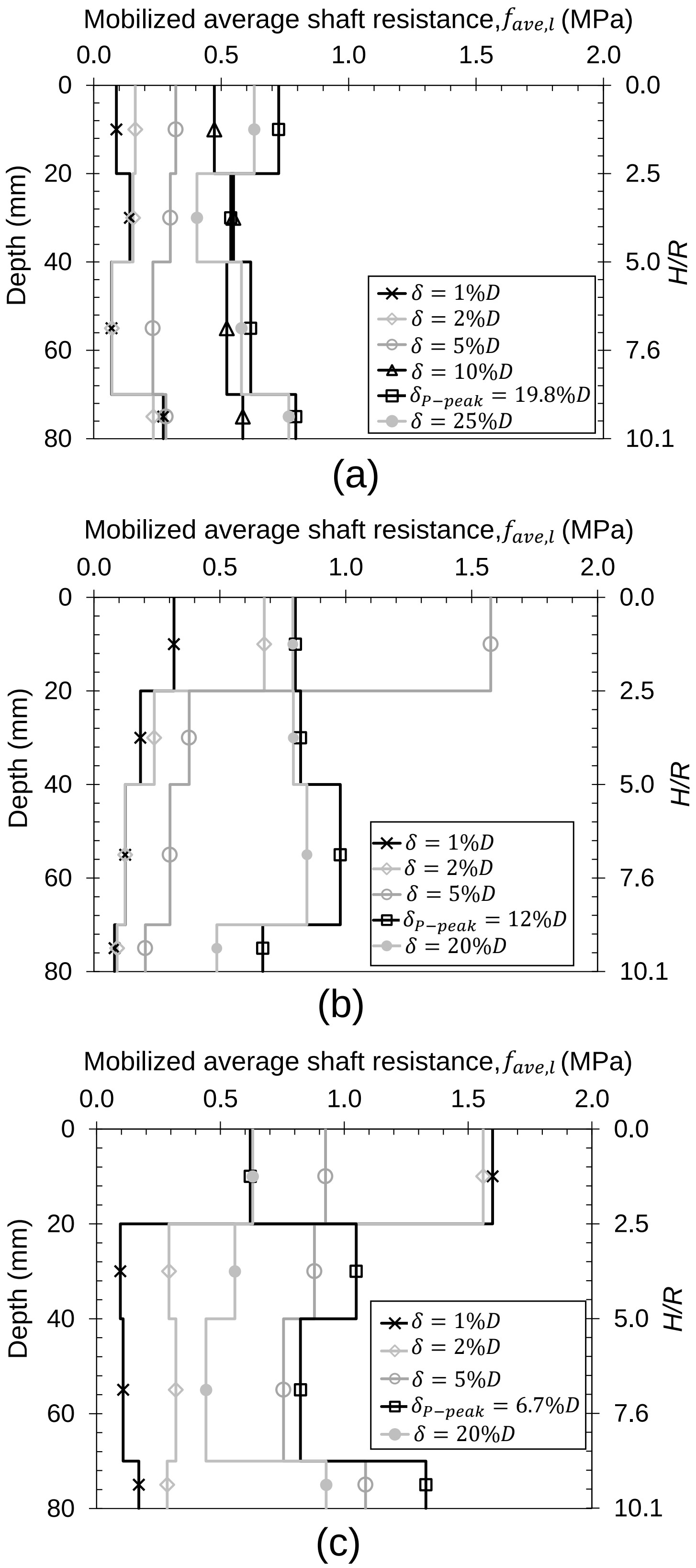

Fig. 9. Mobilized average shaft resistance distribution (vs depth) for a given settlement for centrifuge tests with different roughness profiles: (a) RF= 0.025, (b) RF= 0.050, (c) RF= 0.106.

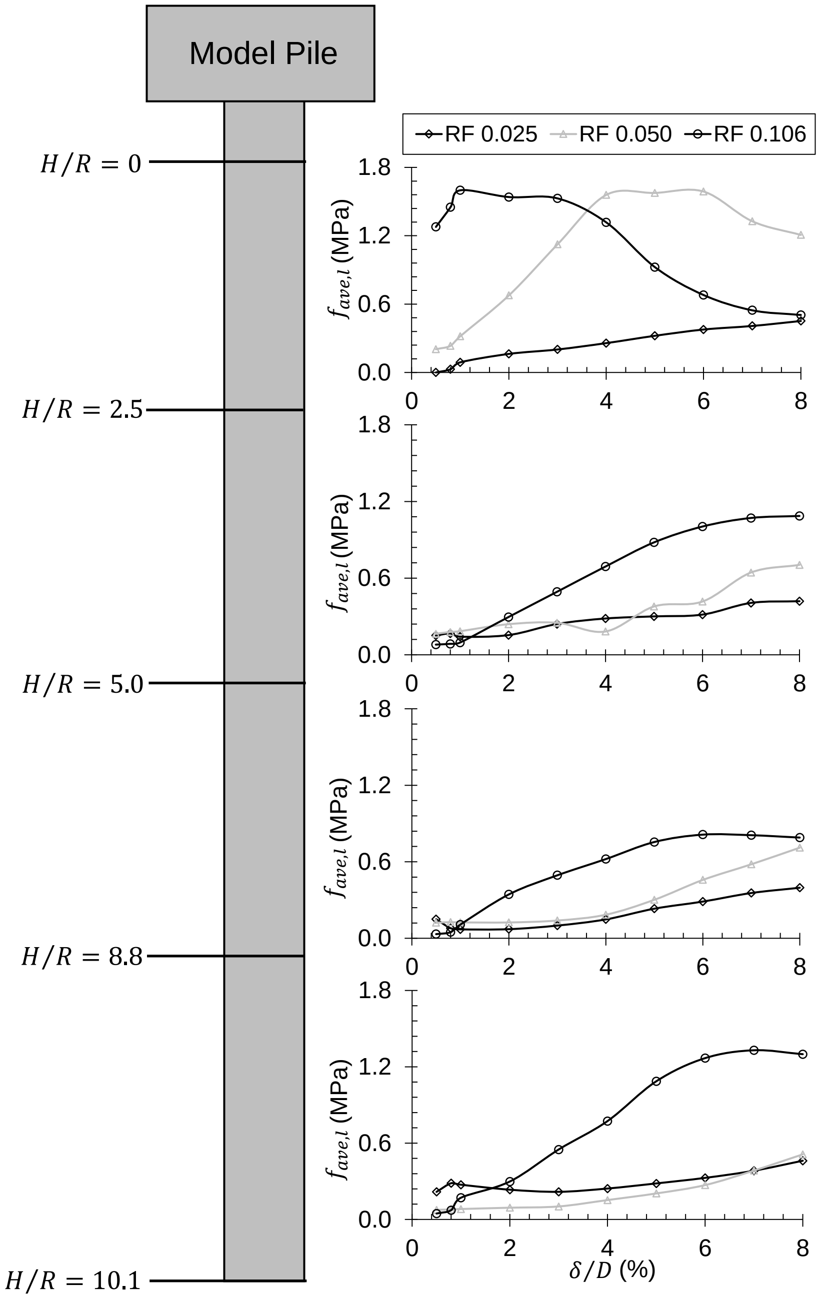

Fig. 10. Mobilized average shaft resistance vs pile head settlement at different depths below the socket for centrifuge tests with different roughness profiles.

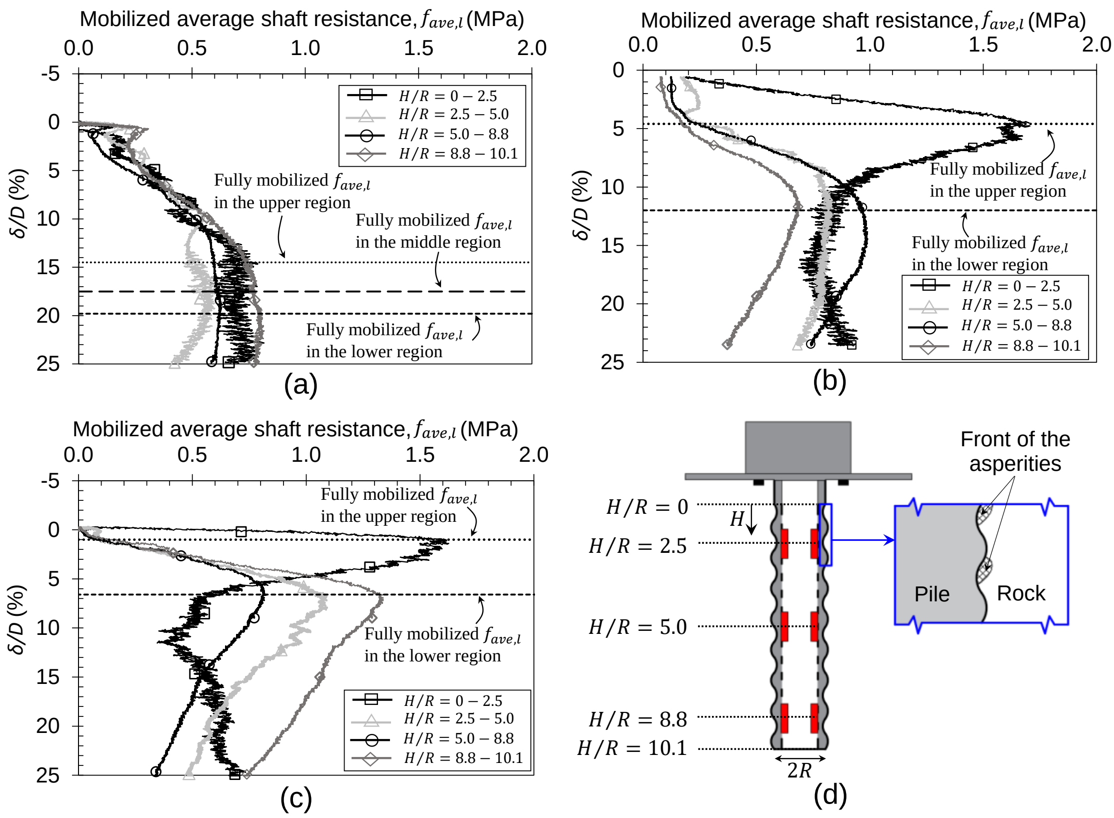

Fig. 11. Mobilized average shaft resistance vs pile head settlement at different depths below the socket for centrifuge tests with different roughness profiles: (a) $RF = 0.025$, (b) $RF = 0.050$, (c) $RF = 0.106$; (d) details of the front of the asperities.

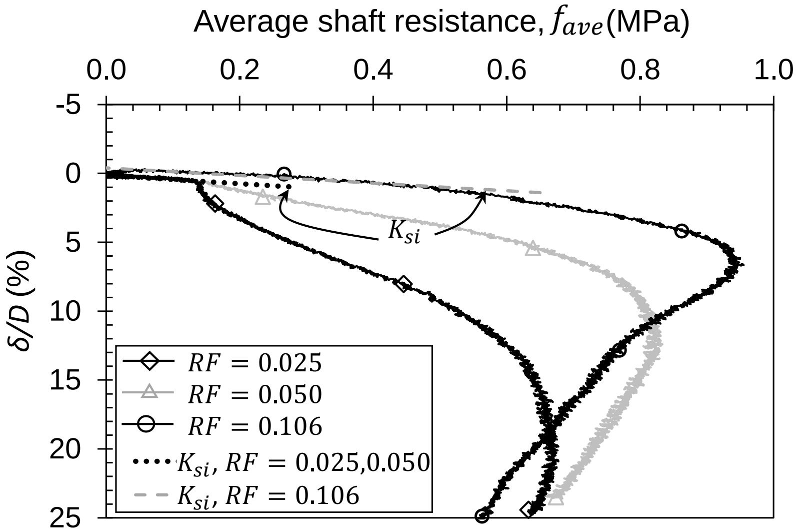

Fig. 12. Average shaft resistance-settlement curves of centrifuge tests of rock-socketed piles with polystyrene base and different roughness profiles.

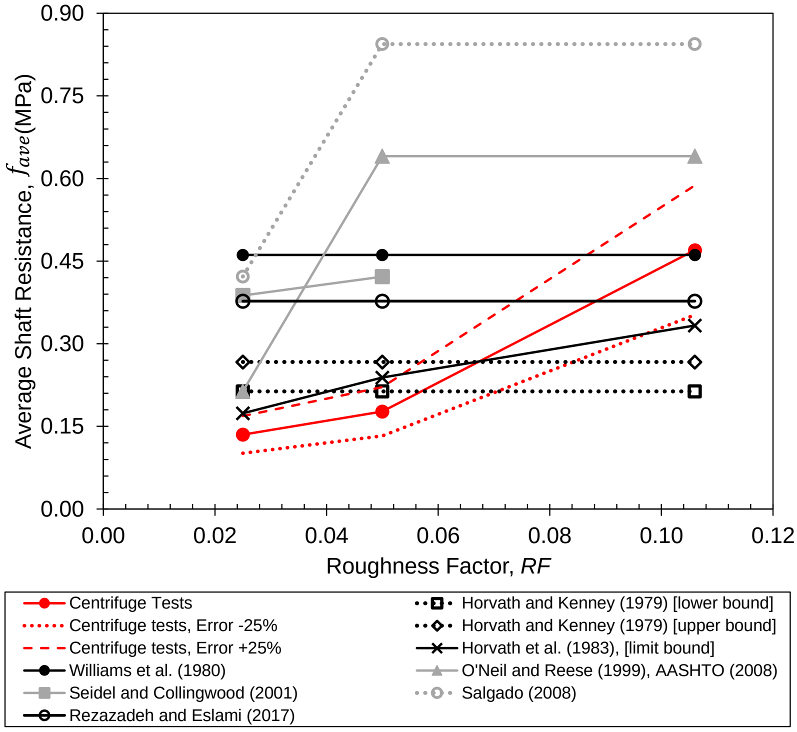

Fig. 13. Shaft resistance estimation: comparative between centrifuge tests results and empirical and analytical criteria.